IIETA International Information and Engineering Technology Association
Advancing the World of Information and Engineering

Annales de Chimie - Science des Matériaux
Vol. 50, No. 1, February, 2026, pp. 13-22
Journal homepage: http://iieta.org/journals/acsm

Effect of Calcium Fluoride (CaF_2) Additions on the Microstructure, Physicomechanical Performance, and Ion-Release Behavior of High-Copper Dental Amalgam

Alaam Ihsan Hadi*, Haydar Jamal Al-Deen

Metallurgical Engineering Department, College of Materials Engineering, University of Babylon, Babylon 51001, Iraq

Corresponding Author Email: alaamihsan979@gmail.com

https://doi.org/10.18280/acsm.500102

Received: 24 November 2025
Revised: 30 January 2026
Accepted: 8 February 2026
Available online: 28 February 2026

Keywords:
dental amalgam, high-copper amalgam, calcium fluoride, microstructure, compressive strength, hardness, creep, dimensional change

ABSTRACT

Dental amalgam remains a reliable posterior restorative material in many settings despite global mercury phase-down policies. This study evaluates CaF_2-modified high-copper dental amalgam within a controlled composition window (0.5–3.0 wt%) using an integrated microstructure–property–release approach, while maintaining specimen integrity. Phase constitution and microstructural features were characterized by X-ray diffraction (XRD), scanning electron microscopy with energy-dispersive spectroscopy (SEM-EDS), and Fourier-transform infrared spectroscopy (FTIR), and correlated with American Dental Association (ADA)-standard physicomechanical metrics (dimensional change, compressive strength, hardness, and creep) and with Hg and F^- release under the present in-vitro conditions. One-way analysis of variance (ANOVA) with Holm correction was used for physicomechanical endpoints ($\alpha = 0.05$). XRD confirmed retention of the characteristic set-amalgam phases ($\gamma1$–Ag_2Hg_3 and η–Cu_6Sn_5) and showed CaF_2 reflections, with no additional reaction-derived crystalline phases detected within the instrument's detection limits. Compressive strength and hardness increased with CaF_2 content, while dimensional change and creep decreased, yielding the best overall load-bearing response at 3 wt% CaF_2. Mercury release was lowest at 0.5 wt% CaF_2 (0.0326 ppb; ~99.2% lower than the master alloy, M) under the present protocol. At 3 wt% CaF_2, Hg release approached the SG43 reference. Fluoride release varied with composition. Overall, CaF_2 enables tailoring a practical balance between mechanical performance and Hg/F^- release, depending on the targeted clinical priority.

1. INTRODUCTION

The dental amalgam has been used as a strong direct restorative material in the posterior teeth over the last century due to its high fracture resistance, relative resistance to moisture during placement, and consistent long-term clinical survival in high-load areas [1, 2]. Despite the fact that amalgam is no longer used in a number of markets due to the global phase-down initiatives, which are, in part, driven by the mercury stewardship and environmental policy, amalgam is still clinically relevant in most of the settings where longevity, cost, and operative simplicity continue to play decisive roles [3-5]. In this regard, the materials-engineering approaches, which improve the performance of amalgam and help to mitigate risks are scientifically and clinically significant [6-9].

Metallurgically, the emergence of high-copper amalgams is one of the significant materials innovations to reduce corrosivity-prone phases and enhance mechanical integrity to minimize marginal breakdown and increase long-term service behavior [10]. However, the performance of amalgamation is highly composition- and kinetics-sensitive: even small additions may alter phase composition, microstructure and degradation mechanisms, which have quantifiable effects on mechanical behavior and corrosion-related behavior [11]. In line with other general developments in dental materials, recent studies are increasingly focusing on functional additives, which are typically at the micro- or nano-scale, to strengthen the matrix, control release properties, and enhance degradation resistance, as long as dispersion and interfacial integrity remain properly managed [12].

In this context, calcium fluoride (CaF_2) has been of interest as chemically stable source of fluoride with good biocompatibility and potential longevity of fluoride under the conditions of interest [13]. Fluoride-releasing systems have become the subject of a wide range of research as they have remineralization-adjacent properties and may affect interfacial stability in the oral environment [14]. Additionally, it was reported that CaF_2-based coatings and composites can be coupled to metallic substrates and maintain biocompatible functionality in biomedical applications [15]. These findings encourage the consideration of CaF_2 as an effective additive in metallic restorative matrices, such as high-copper amalgams, in which microstructural/phase transitions can concurrently affect both mechanical behavior and release-related behavior [11].

The current clinical and population-based findings still support the use of amalgam as a restorative choice in challenging posterior signs, and the necessity to have

trustworthy evidence-based materials comparisons in the face of changing policy pressures [2, 6]. Simultaneously, the electrochemical degradation is one of the key determinants of the long-term service behaviour of amalgam; therefore, the microstructure-sensitive corrosion and impedance investigations offer important information on how phase constitution and microstructural heterogeneity control the degradation mechanisms in high-copper systems [10]. Simultaneously, experimental research on particulate modification (e.g., titanium-based reinforcement) show that additive-based amalgam microstructure can be engineered and that mechanical response can be enhanced by additive-based microstructural control is a rational materials-engineering strategy [11]. Collectively, these lines of evidence support systematic, standards-aligned investigations of functional additives in amalgam systems, particularly where both performance and release-related outcomes are relevant.

Nevertheless, systematic studies on using CaF_2 as an additive in high-copper dental amalgam—while explicitly linking phase constitution/microstructural evolution to standardized physicomechanical performance and Hg/F^- release—remain scarce. This knowledge gap motivates the present work.

To address this gap, an integrated microstructure–property–release assessment is presented for CaF_2-modified high-copper dental amalgam within a controlled composition window (0.5–3.0 wt%). Phase constitution and microstructural features, characterized by XRD and scanning electron microscopy with energy-dispersive spectroscopy (SEM-EDS) (with Fourier-transform infrared spectroscopy (FTIR) providing complementary chemical signatures), are correlated with ANSI/ American Dental Association (ADA)-standard physicomechanical metrics (dimensional change, compressive strength, hardness, and creep) and with mercury and fluoride release under the present in-vitro conditions.

Accordingly, this study evaluates how incremental CaF_2 additions (0.5–3.0 wt%) affect the phase constitution and microstructural evolution of high-copper dental amalgam, and how these changes translate into ADA-standard physicomechanical performance and Hg/F^- release under the present in-vitro conditions. It is hypothesized that low-to-moderate CaF_2 additions can maintain or improve physicomechanical properties through microstructural refinement and altered phase distribution, while measurably influencing Hg and F^- release, with an optimum CaF_2 level balancing performance and release behavior. To test this, phases and additive-related signatures are characterized (XRD/SEM-EDS/FTIR), ADA-standard physicomechanical properties are quantified, and mercury and fluoride release are measured under the present testing conditions.

2. MATERIALS AND METHODS

2.1 Alloy fabrication and groups

A high-copper dental amalgam alloy having a nominal composition of Ag: 48 wt%, Sn: 30 wt%, Cu: 21 wt% and Zn: 1wt% was used as the base alloy which was prepared in this study. The constituent metals were first melted in a gas furnace under an inert argon atmosphere to prevent oxidation; the molten alloy-metal was cast as ingots with a custom-made steel casting template to provide repeatable geometry (Figure 1(a)). It is comprised of two tightly clamped blocks containing a cylindrical cavity to self-locate them during pouring and minimize dimensional variation from cast to cast (Figure 1(a)). After solidification, the produced ingots exhibited a uniform elongated shape suitable for subsequent cutting and specimen preparation (Figure 1(b)).

The selected CaF_2 additions (0.5, 1.0, 1.5, 2.0, 2.5, and 3.0 wt%) were designed to probe a low-to-moderate composition window in which measurable effects on microstructure and fluoride availability can be captured, while minimizing the risk of particle agglomeration, micro-defect formation, and deterioration of load-bearing physicomechanical properties. This window facilitates identifying an optimum trade-off between ADA-standard physicomechanical performance and Hg/F^- release under the present in-vitro conditions.

Figure 1. Casting mold and ingot (a) Steel mold. (b) As-cast ingot

Table 1. Nominal chemical composition (wt%) of the fabricated high-copper base alloy and the commercial reference alloy (SG43)

Alloy	Ag (wt%)	Sn (wt%)	Cu (wt%)	Zn (wt%)
Base Alloy (M)	48.12	30.88	21.06	0.6208
SG43	43	32	25	-

As shown in Table 1, the nominal chemical composition of the fabricated high-copper base alloy was compared with that of the commercial reference alloy (SG43). This composition window also represents a practical screening range for minor additive modification of amalgam, enabling quantitative evaluation of composition-dependent changes in compressive strength, hardness, dimensional change, and creep, together with Hg and F^- release, while maintaining adequate processability and specimen integrity for standardized ADA testing [16].

2.2 Preparation of specimens

The specimens were prepared measured according to ADA Specification No.1 with equal weights of alloy powder and mercury triturated for 25 s on an electrically driven amalgamator (Ling Chen type) [10]. The freshly prepared alloy was condensed in cylindrical molds producing samples with 4 mm diameter at base and 8 mm high (1:2), which were stored at 37 ± 1 °C before testing [10, 11]. A dedicated specimen preparation mold assembly was employed to generate replicable geometry and compaction conditions (Figure 2). Using mold components (split mold, plungers and locking parts) to pack the molds with controlled pressure provides uniform dimension of the test specimens, increasing test repeatability by reducing geometric variability within

groups (Figure 2). Five specimens were tested per group (n = 5), which is consistent with common practice in dental materials research and supports reliable estimation of variability under laboratory conditions [11]. Data are presented as mean ± standard deviation (n = 5).

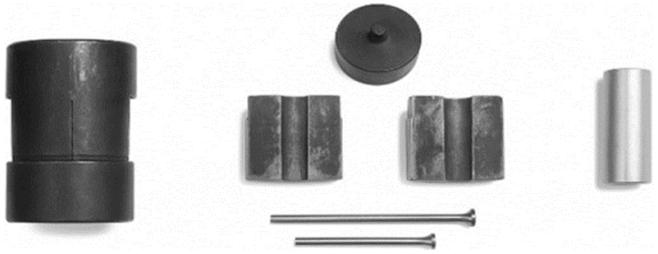

Figure 2. Components of the specimen preparation mold assembly used to produce standardized cylindrical amalgam specimens for mechanical testing

2.3 Characterization

2.3.1 X-ray diffraction analysis

Phase identification was performed by X-ray diffraction (XRD) for the base alloy precursor, the commercial reference amalgam (SG43), the master amalgam (M), and the 3 wt% CaF_2-modified group (M + 3 wt% CaF_2). Measurements were carried out using a SHIMADZU LabX XRD-6000 diffractometer with Cu Kα radiation (λ = 1.5406 Å) and a nickel filter. Diffraction patterns were recorded over a 2θ range of 30°–80°.

2.3.2 Microstructural observation and elemental analysis

Microstructural characterization was conducted for the base alloy (before and after homogenization heat treatment) and for the amalgam groups (including CaF_2 additions). Specimens were ground sequentially using SiC abrasive papers of 400, 600, 800, 1200, 1500, 2000, and 2500 grit, followed by polishing with 3 μm diamond paste. After polishing, specimens were rinsed thoroughly with distilled water, dried using an air stream, and then etched using a chemical solution prepared by mixing 5 mL of nitric acid with 95 mL of distilled water. SEM imaging was performed to examine the morphology and microstructural features, while EDS analysis and elemental mapping were used to assess compositional distribution and confirm the presence and dispersion of Ca- and F-containing regions in CaF_2-modified samples.

2.4 Physicomechanical tests

A total of five samples were prepared and tested in each group (n = 5). Unless specified otherwise, samples were conditioned at 37 ± 1 °C before testing to achieve a similar setting and conditioning condition.

2.4.1 Dimensional change

Dimensional stability was tested at 37 ± 1 °C in water bath with constant temperature according to ADA Specification No. 1. The initial measurement was recorded 30 min after mixing to capture early-stage dimensional behavior after initial setting stabilization. The final measurement was conducted after 24 h under the same temperature conditions. Dimensional variation was assessed against the standard requirement, where the dimensional change should remain within ± 20 μm/cm.

2.4.2 Compressive strength

Compressive strength was measured using a universal testing machine (Instron, model WDW-200) at a crosshead speed of 0.5 mm/min. cylindrical specimens (4 mm in diameter and 8 mm in height) were positioned vertically and loaded axially until failure, consistent with a uniaxial compression configuration (Figure 3). Specimens were tested at two time points (1 day and 7 days after mixing), and all samples were maintained at 37 ± 1 °C prior to testing. The mean compressive strength for each group was calculated from five replicates (n = 5).

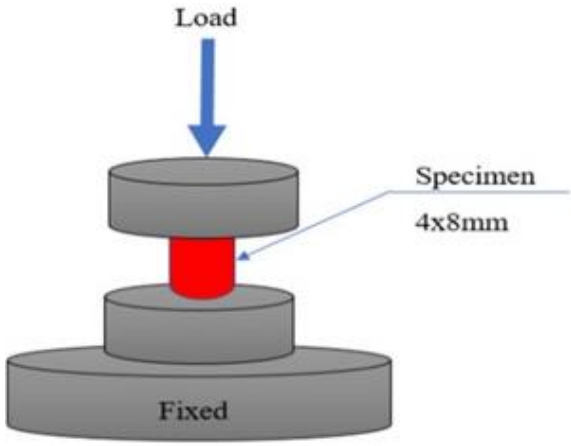

Figure 3. Schematic illustration of the uniaxial compression test configuration for cylindrical specimens (4 mm × 8 mm), showing axial loading and fixed support

2.4.3 Vickers hardness test

Vickers microhardness was measured using a digital microhardness tester (model TH715). A load of 200 gf was applied for 10 s, and hardness was determined from the diagonal lengths of the indentation. Measurements were performed at two post-mixing time points (1 day and 7 days). For each specimen, multiple indentations were placed at separated locations to avoid interaction of plastic zones, and the average hardness value was calculated for each group.

2.4.4 Creep test

Creep testing was conducted in accordance with ADA Specification No. 1 at 37 ± 1 °C. Cylindrical specimens (4 mm × 8 mm) were subjected to a constant uniaxial compressive stress of 10 MN/m², applied using the loading configuration illustrated in Figure 4. The specimen length was measured using a micrometer caliper 3 h after amalgamation, then the load was maintained for 21 h, after which the final length was recorded. Creep (%) was calculated from the change in specimen length under sustained load relative to the initial length, and results were reported as the mean of five specimens per group (n = 5).

2.5 Mercury vapor and ion release

To assess release-related behavior of the investigated amalgam systems under simulated oral conditions, both mercury release and fluoride ion release were evaluated. These tests provide complementary information on material–environment interaction, including potential exposure-related behavior and functional ion availability associated with CaF_2 incorporation.

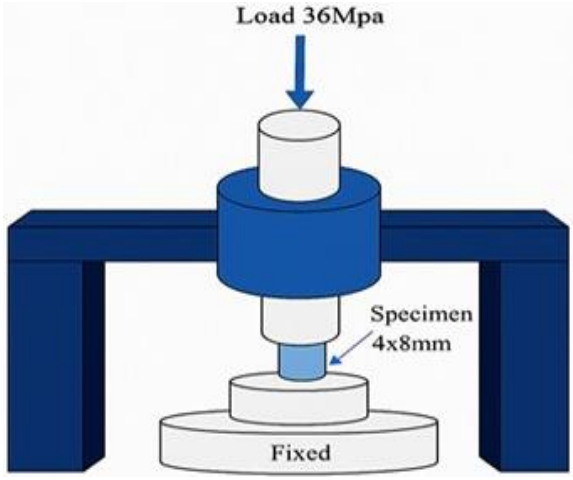

Figure 4. Schematic illustration of the creep test configuration for cylindrical amalgam specimens (4 mm × 8 mm) under constant uniaxial compressive loading at 37 ± 1 ℃

2.5.1 Mercury release test

Mercury release from the investigated amalgam groups (with and without CaF_2 additions) was evaluated using a static immersion protocol in artificial saliva. The test followed relevant guidance for metallic biomaterials (JIS T-0304), where specimens were immersed individually in sealed plastic containers containing 100 mL of artificial saliva for 30 days at 37 ± 1 ℃ inside a temperature-controlled chamber [17, 18]. Mercury concentration in the immersion medium was determined using the mercury-analysis instrument shown in Figure 5, following instrument calibration and blank correction. The use of controlled immersion volume, sealed containers, and fixed temperature conditions was intended to minimize test-to-test variability and enable reliable comparison of mercury release among groups [17, 18].

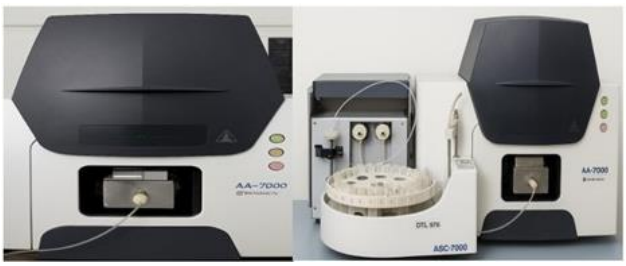

Figure 5. Mercury release measurement system used to quantify mercury concentration in immersion media following static exposure of amalgam specimens in artificial saliva

Figure 6. Experimental setup for fluoride ion release measurement using a fluoride ion-selective electrode (ISE), including calibration and sample measurement arrangement

2.5.2 Fluoride ion release test

Fluoride ion release was quantified by immersing standardized specimens in deionized water or artificial saliva and measuring fluoride concentration at specified time intervals using a fluoride ion-selective electrode (ISE). The measurement system and bench setup are shown in Figure 6. Prior to measurements, the electrode was calibrated using fluoride standard solutions, and total ionic strength adjustment buffer (TISAB) was added to samples to stabilize ionic strength and pH during ISE measurements [18, 19]. The storage medium was renewed as required to maintain sink conditions, and fluoride release values were reported as concentration (ppm) and/or normalized to specimen surface area (μg/cm²), depending on the reporting format adopted [18, 19].

2.6 Statistical analysis

Inferential statistics were performed in addition to reporting mean ± SD and 95% CI. Normality and homogeneity of variances were assessed using the Shapiro–Wilk and Levene tests, respectively. For each physicomechanical endpoint, One-way analysis of variance (ANOVA) was applied to test for overall group differences ($\alpha = 0.05$). Post-hoc comparisons versus the unmodified control (M) were then conducted using pooled-variance t-tests with Holm correction to control the familywise error rate. If normality or variance-homogeneity assumptions were violated, the Kruskal–Wallis test (with appropriate post-hoc multiple comparisons) was used. Release measurements (Hg and F^-) are reported descriptively as measured concentrations under the stated protocol; therefore, inferential statistics were not applied to release endpoints. Reported p-values correspond to the inferential analyses described above.

2.6.1 Arithmetic mean

The arithmetic mean, or average, is the total of a set of numbers divided by the number of values in that set. The collection frequently constitutes a compilation of experimental outcomes [20].

$$\bar{x} = \frac{\sum x}{n} \tag{1}$$

where,

X = arithmetic mean

n = number of values.

2.6.2 Standard deviation

The standard deviation was computed via the formula [17].

$$s^2 = \frac{1}{n-1}\sum_{j=1}^{n}(x_j - \bar{x})^2 = \frac{1}{n-1}[x_1 - \bar{x})^2 + \cdots + (x_n - \bar{x})^2 \tag{2}$$

where,

S^2 = standard deviation

x = individual value

$\bar{x}$ = arithmetic mean

n = number of the values.

2.6.3 Confidence interval (CI)

The confidence interval is a statistical measure that specifies the range that one would expect the true mean of the dataset to lie in, say with 95% confidence. A 95% confidence interval (95% CI) means that there is a 95% chance that the true mean lies within this range. The formula uses the average, standard deviation, and sample size [21].

$$\frac{S}{\sqrt{n}} \times t_{a/2,n-1} \pm \bar{x} = CI \quad (3)$$

where,

$\bar{x}$ = arithmetic mean

S = standard deviation

n = number of samples

3. RESULTS

3.1 Microstructure characterization

XRD pattern (Figure 7) for the base alloy, reveals that three intermetallic phases exist in the as-cast alloy; γ (Ag_3Sn), ε(Cu_3Sn) and β(Ag_4Sn). The γ (Ag_3Sn) phase is the major matrix component in the base alloy, and it can be attributed by the most acute reflections at 2θ = 34.24°, 37.30°, and 39.27°. The ε(Cu_3Sn) phase was identified as a secondary phase, which is basically Cu–Sn intermetallic lattice of the system with Bragg peaks at 2θ = 42.82°, 51.89° and 62.25°. Weaker reflections related with β (Ag_4Sn) phase are also indexed at 2θ =41.44°, 69.35°, 75.17° and 76.45°indicating the existence of low fraction of β-phase relative to γ and ε phases. In general, the relative peak intensities of the microstructure (map) in Figure 7 indicate a γ-controlling with second ε and third β phase-forming constituents type. Notice that Figure 7 refers to the phase constitution of the precursor base alloy before mercurial contact and thus it corresponds to the outset intermetallic skeleton prior amalgamation.

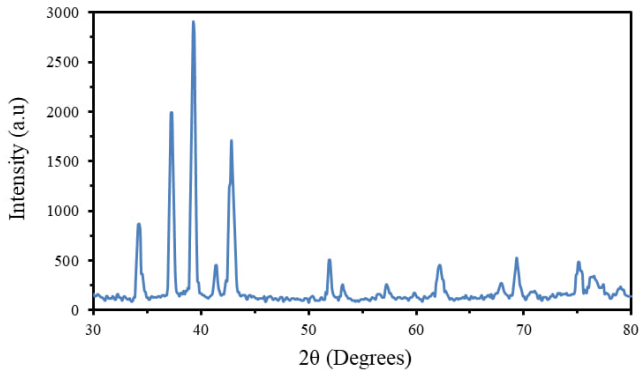

Figure 7. XRD pattern of the fabricated base alloy (precursor) showing indexed reflections corresponding to γ-Ag_3Sn, ε-Cu_3Sn, and β-Ag_4Sn phases; the dominant γ-Ag_3Sn peaks occur at 2θ = 34.24°, 37.30°, and 39.27°

The XRD pattern of the master amalgam (Figure 8) confirms the formation of the characteristic amalgamation reaction products after setting. Two principal phases are identified and indexed in the diffractogram: the γ1 phase (Ag_2Hg_3) and the η phase (Cu_6Sn_5). The γ1-Ag_2Hg_3 phase constitutes the dominant mercury-containing matrix that develops during the reaction of the alloy powder with mercury. Its indexed reflections are observed at 2θ = 32.84°, 36.96°, 47.27°, 64.09°, 69.11°, and 71.30°. In parallel, the η-Cu_6Sn_5 phase is detected as a Cu–Sn reaction product typical of high-copper amalgam systems, reflecting the participation of copper in the setting reaction. The indexed η-Cu_6Sn_5 reflections appear at 2θ = 31.37°, 34.85°, 39.41°, 41.99°, 42.44°, 44.89°, 46.05°, 48.11°, 54.52°, and 58.71°. In general, the presence and indexing of γ1-Ag_2Hg_3 as well as η-Cu_6Sn_5 in Figure 8 confirm that the control amalgam contains the anticipated phase composition after having been amalgamated under these processing conditions.

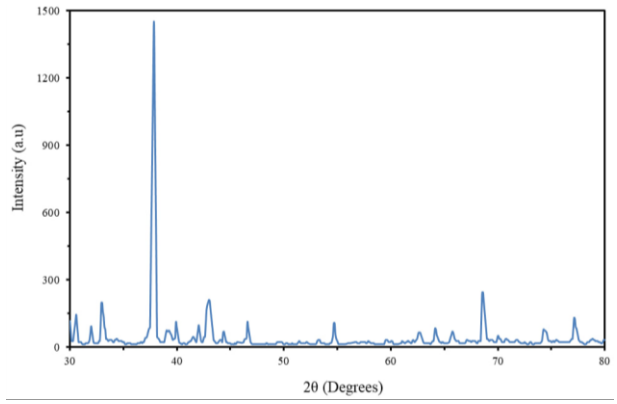

Figure 8. XRD pattern of the master amalgam showing characteristic amalgamation reaction products (γ₁-Ag_2Hg_3 and η-Cu_6Sn_5)

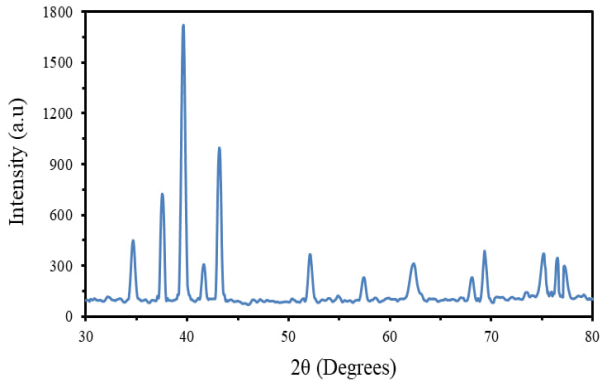

Figure 9. XRD pattern of the set amalgam containing 3 wt% CaF_2, showing the retained amalgamation products γ₁-Ag_2Hg_3 (2θ = 37.55°, 41.66°, 43.18°, 57.42°, 75.17°, 77.22°) and η-Cu_6Sn_5 (2θ = 62.38°, 67.82°, 69.34°, 76.56°), together with additional reflections assigned to CaF_2 (2θ = 34.70°, 39.67°, 52.12°)

When 3 wt% CaF_2 is added, the onset of the principal alloying reaction products is observed on the XRD pattern shown in Figure 9 where the reflection associated with γ₁ (Ag_2Hg_3) and η (Cu_6Sn_5) remain visible. The γ₁-(Ag_2Hg_3) phase is identified by peaks at 2θ = 37.55°, 41.66°, 43.18°, 57.42°, 75.17°, and 77.22°, while the η-(Cu_6Sn_5) phase is confirmed by reflections at 2θ = 62.38°, 67.82°, 69.34°, and 76.56°. Unlike the patterns observed for master amalgam (Figure 8), in Figure 9, there are new diffraction reflections derived from the addition of CaF_2, which arise at 2θ = 34.70°, 39.67° and at 52.12°; these peaks show that in the prepared amalgam we have CaF_2 as a separate crystalline phase included within it. Most importantly, the presence of both the γ1/η phases along with CaF_2 related peaks indicate that CaF_2 does not inhibit the major setting reaction products, and that it

includes in the microstructures another phase.

The XRD results support a multiphase set-amalgam microstructure dominated by γ1 (Ag_2Hg_3), which forms the primary Hg-containing matrix and contributes to overall cohesion, and η (Cu_6Sn_5), a typical Cu–Sn transformation product in high-copper systems that is associated with strengthening and improved wear resistance. The presence of retained CaF_2 reflections is consistent with additive retention and provides a structural basis for discussing composition-dependent release behavior and microstructural evolution. These phase-level observations are complemented by the microstructural evidence presented in Figures 10-12.

Microstructural evolution of the investigated system is illustrated across three sequential material states: (i) the as-fabricated base alloy precursor prior to mercury exposure (Figure 10), (ii) the master amalgam after setting/amalgamation with mercury (Figure 11), and (iii) the CaF_2-modified amalgam, where additive-retention signatures are evident (Figure 12). This sequence highlights the influence of precursor homogenization on subsequent microstructural and phase development during amalgamation and clarifies the additional features associated with CaF_2 incorporation.

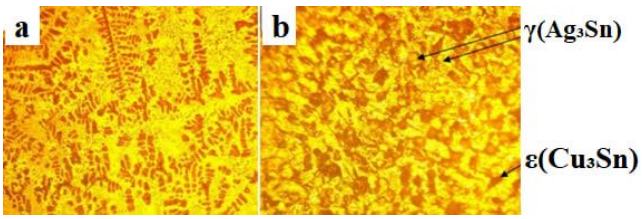

Figure 10. Optical micrographs of the fabricated base alloy illustrating the effect of homogenization heat treatment: (a) prior to homogenization and (b) after homogenization, highlighting the distribution of γ (Ag_3Sn) and ε (Cu_3Sn) constituents

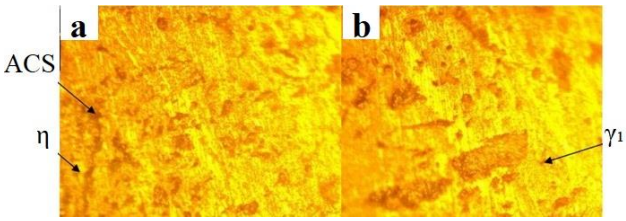

Figure 11. Optical micrographs of the master amalgam after amalgamation (setting) at different magnifications: (a) 200× overview showing residual unreacted alloy particles (ACS; Ag–Cu–Sn) and η′ regions, and (b) 600× micrograph emphasizing the γ_1 (Ag_2Hg_3) matrix region

Figure 10(a) and (b) illustrates the microstructure of the fabricated base alloy and the effect of homogenization heat treatment. Prior to homogenization (Figure 10(a)), the microstructure shows a comparatively heterogeneous morphology, consistent with local compositional gradients and segregation inherited from fabrication/solidification. After homogenization (Figure 10(b)), the microstructure becomes more uniform, reflecting a reduction in compositional inhomogeneity and a more balanced distribution of the alloy constituents. The annotated phases/constituents (γ, Ag_3Sn and ε, Cu_3Sn) are typical intermetallic features of the precursor alloy and serve as a baseline for interpreting the subsequent amalgamation stage. Importantly, Figure 10 represents the alloy before reaction with mercury; therefore, mercury-containing reaction products are not expected at this stage.

Figure 11(a) and (b) characterizes the master amalgam after amalgamation (setting) and therefore represents a fundamentally different microstructural state than Figure 10. At lower magnification (200×, Figure 11(a)), the microstructure is representative of the set material and allows for an overview of: space distribution between regions corresponding to the set matrix; and unreacted alloy particles (ACS: Ag–Cu–Sn). These unreacted particles are evidence of incomplete consumption of the precursor alloy and are usually encapsulated by reaction zones. The identical image also shows η′ zones, indicating that Cu–Sn reaction products precipitate in copper-containing amalgam systems and affect the mechanical and corrosion-related response. At higher magnification (Figure 11(b), 600×), the microstructure shows the γ_1(Ag_2Hg_3)-dominant matrix region as a major load-carrying phase after setting. This difference between Figure 11(a) and (b) is intentional: the former is the most suitable for microscale evaluation of phase/constituent distribution, while the latter yields greater clarity on matrix control and local segregation close to residual particles.

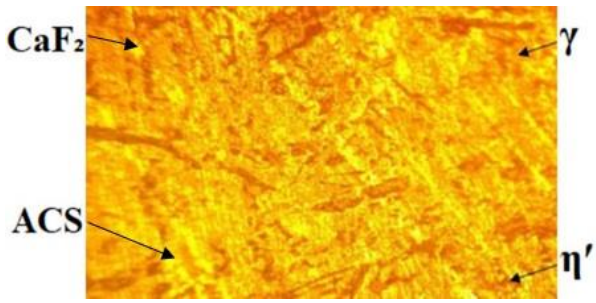

Figure 12. Optical micrograph of the 3 wt% CaF_2-modified amalgam (400×) showing CaF_2-associated regions/particles within the set microstructure, together with the labeled γ matrix, η′ regions, and residual ACS particles

Figure 11 illustrates the microstructure of unmodified master amalgam (400×), which can be compared directly with the 3 wt% CaF_2-amalgam (Figure 12). Aside from features already present in the master amalgam, i.e. the labeled γ matrix, η′ regions and residual ACS particles, Figure 12 also exhibits CaF_2 related regions/particles that provide a visual marker for additive inclusion into the microstructure. The existence of these regions shows that some portion of CaF_2 does not dissolve or vanish completely into the microstructure during processing. Accordingly, in Figure 12, there appears a CaF_2-related microstructural feature (inherited from the modified system) superimposed on the fingerprint of the master amalgam's microstructure.

3.2 Dimensional change (expansion) test

Dimensional change (in μm/cm, positive values indicate expansion). Two reference groups that were not manipulated were assessed: SG43, a dental amalgam purchased from a commercial source, and M, the master (base) alloy. The expansion of SG43 was +12.52 μm/cm, and the expansion of M was +14.88 μm/cm. The alloy system was then paired with CaF_2 (at 0.5–3 wt%) to evaluate the effect of the additive in modified groups versus both of the references (M and SG43). A clear concentration-dependent reduction in expansion was observed with increasing CaF_2 content, decreasing from

+10.40 µm/cm at 0.5 wt% to +8.90, +7.12, +6.67, +4.02, and +3.01 µm/cm at 1, 1.5, 2, 2.5, and 3 wt%, respectively. This gradual decrease indicates better dimensional stability. Simultaneously, the improving percentages listed in Table 2 were raised in a monotonic manner from 30.10% (0.5 wt%) to 40.20% (1 wt%), 52.14% (1.5 wt%), 55.18% (2 wt%), 72.97% (2.5 wt%) and 79.78% (3 wt%), further predicting the benefit of the CaF_2 addition. The corresponding 95% confidence intervals for all groups show that the trend measured is consistent. One-way ANOVA across the eight groups (SG43, M, and the six CaF_2-modified compositions) indicated significant differences among groups ($F(7,32) = 38.81$, $p < 0.001$). Holm-adjusted pairwise comparisons versus the unmodified control (M) were significant for all CaF_2-containing groups (adjusted $p < 0.001$).

Table 2. Dimensional change results (µm/cm) of the investigated dental amalgam alloys and CaF_2-modified groups, reported as mean SD with the corresponding 95% confidence interval (95% CI)

Alloys	Dimensional Change (µm/cm)	Mean SD	95% CI	Improvement (%)
SG43	+12.52 µm/cm	1.3	11.02 – 14.02	-
M	+14.88 µm/cm	0.50	14.26 – 15.50	-
M + 0.5% CaF_2	+10.40 µm/cm	2.4	7.37 – 13.43	30.10%
M + 1% CaF_2	+8.90 µm/cm	1.0	7.66 – 10.14	40.20%
M + 1.5% CaF_2	+7.12 µm/cm	1.6	4.91 – 9.33	52.14%
M + 2% CaF_2	+6.67 µm/cm	2.1	3.41 – 9.93	55.18%
M + 2.5% CaF_2	+4.02 µm/cm	0.78	3.10 – 4.94	72.97%
M + 3% CaF_2	+3.01 µm/cm	0.9	1.89 – 4.13	79.78%

3.3 Compressive strength

Compressive strength (MPa) of the unmodified (M, reference and SG43) and CaF_2-modified groups (0.5–3 wt%) were shown for two aging times; 1, and 7 d in Table 3. As expected, the maturation strength gain was observed for the M alloy, as its compressive strength at 7 days (53.975 MPa) after mixing exceeded that at 1 day (42.8 MP). The CaF_2 modified samples also showed a concentration dependent increase at both time points. The average strength of the 0.5 wt% reached a value of 52.1 Mpa after 1 day while for other samples these values are; 56.4 MPa (for 1 wt%), 60.2 MPa (for 1.5 wt%), 64.3 MPa (for 2 wt%), 69,1 MPa (for 2.5 wt%) and then 73.4 MPa (for 3 wt%). After 7 days, the same trend persisted, rising from 80.5 MPa (0.5 wt%) to 87.2 MPa (1 wt%), 92.0 MPa (1.5 wt%), 97.3 MPa (2 wt%), 112.8 MPa (2.5 wt%), and reaching 121.4 MPa at 3 wt% CaF_2. Variability is summarized in the table as standard deviation (SD), while the 95% confidence interval (95% CI) is provided for the 7-day values to indicate the precision of the estimates. The improvement percentage listed in the final column represents the increase in 7-day compressive strength relative to the master alloy (M) and increased monotonically from 21.8% (0.5 wt%) to 30.84% (1 wt%), 40.19% (1.5 wt%), 49.53% (2 wt%), 61.21% (2.5 wt%), and 70.56% (3 wt%), confirming the strengthening effect of CaF_2 addition over the studied range. The 7-day compressive strength differed significantly among groups (one-way ANOVA: $F(7,32) = 1150.3$, $p < 0.001$). Holm-adjusted pairwise comparisons versus the unmodified control (M) were significant for all CaF_2-modified compositions (adjusted $p < 0.001$).

Table 3. Compressive strength (MPa) of the investigated dental amalgam groups measured after 1 and 7 days

Alloys	1 Day	Mean SD	7 Days	Mean SD	95% CI	Improvement (%)
M	42.8 MPa	2.13	53.975	1.65	-	-
SG43	39.3 MPa	1.9	46.9 MPa	1.4	-	-
M + 0.5% CaF_2	52.1 MPa	2.1	80.5 MPa	1.8	78.3–82.7	21.8%
M + 1% CaF_2	56.4 MPa	1.2	87.2 MPa	2.2	84.5–89.9	30.84%
M + 1.5% CaF_2	60.2 MPa	1.5	92.0 MPa	1.3	90.4–93.6	40.19%
M + 2% CaF_2	64.3 MPa	1.19	97.3 MPa	2.6	94.1–100.5	49.53%
M + 2.5% CaF_2	69.1 MPa	1.1	112.8 MPa	1.01	111.55–114.05	61.21%
M + 3% CaF_2	73.4 MPa	0.91	121.4 MPa	1.1	120.0–122.8	70.56%

Table 4. Vickers hardness $HV_{0.2}$ of the investigated dental amalgam groups measured after 1 and 7 days

Alloys	1 Day	Mean SD	7 Days	Mean SD	95% CI	Improvement (%)
SG43	93.128 Kg/mm^2	2.9	101.59 Kg/mm^2	1.28	100.31 – 102.87	-
M	111.7 Kg/mm^2	1.5	125.39 Kg/mm^2	1.7	123.68 – 127.10	-
M + 0.5% CaF_2	123.5 Kg/mm^2	1.4	137.2 Kg/mm^2	1.7	135.47 – 138.93	10.6%
M + 1% CaF_2	128.1 Kg/mm^2	0.9	172.7 Kg/mm^2	1.2	171.50 – 173.90	14.7%
M + 1.5% CaF_2	135.6 Kg/mm^2	0.6	181.04 Kg/mm^2	1.3	179.74 – 182.34	21.4%
M + 2% CaF_2	142.7 Kg/mm^2	1.1	191.6 Kg/mm^2	1.5	190.04 – 193.16	27.7%
M + 2.5% CaF_2	153.2 Kg/mm^2	2.1	209.1 Kg/mm^2	1.2	207.73 – 210.47	37.1%
M + 3% CaF_2	166.8 Kg/mm^2	1.9	236.2 Kg/mm^2	1.1	235.10 – 237.30	49.3%

3.4 Vickers hardness test

Table 4 presents the Vickers hardness results of the investigated groups, including the two unmodified references—SG43 and M—and the CaF_2-modified specimens (0.5–3 wt%), measured after 1 and 7 days. Hardness increased with aging for both reference groups, rising from 93.13 to 101.59 kg/mm² for SG43 and from 111.7 to 125.39 kg/mm²

for M, consistent with progressive setting and maturation. Incorporation of CaF_2 produced a clear, concentration-dependent increase in hardness at both time points. After 1 day, the mean hardness increased from 123.5 kg/mm² at 0.5 wt% to 128.1, 135.6, 142.7, 153.2, and 166.8 kg/mm² at 1, 1.5, 2, 2.5, and 3 wt%, respectively. The same trend was more pronounced after 7 days, increasing from 137.2 kg/mm² (0.5 wt%) to 172.7, 181.04, 191.6, 209.1, and reaching 236.2 kg/mm² at 3 wt% CaF_2. Dispersion is reported as standard deviation (SD), and the 95% confidence interval (95% CI) is provided for the 7-day values to indicate the precision of the estimates. The improvement percentage listed in the final column represents the increase in 7-day hardness relative to the master alloy (M), rising monotonically from 10.6% (0.5 wt%) to 14.7% (1 wt%), 21.4% (1.5 wt%), 27.7% (2 wt%), 37.1% (2.5 wt%), and 49.3% (3 wt%), confirming the strengthening effect of CaF_2 addition over the investigated range. The 7-day hardness differed significantly among groups (one-way ANOVA: $F(7,32) = 5270.8$, $p < 0.001$); Holm-adjusted pairwise comparisons versus the unmodified control (M) were significant for all CaF_2-modified compositions (adjusted $p < 0.001$).

3.5 Creep test

Table 5 presents the creep results expressed as a percentage (%), where lower values indicate improved resistance to time-dependent deformation. The commercial amalgam (SG43) exhibited a mean creep of 1.11%, whereas the master alloy (M) showed a lower creep of 0.907%. Incorporation of CaF_2 produced a clear, concentration-dependent reduction in creep, decreasing from 0.809% at 0.5% CaF_2 to 0.620% (1%), 0.543% (1.5%), 0.407% (2%), 0.366% (2.5%), and reaching 0.288% at 3% CaF_2. Accordingly, the improvement percentage reported in the table increased progressively with CaF_2 content, from 10.8% at 0.5% to 31.63% (1%), 40.13% (1.5%), 55.12% (2%), 57.62% (2.5%), and 68.25% at 3%, confirming the enhanced creep resistance of the modified groups. Dispersion is summarized as standard deviation (SD), and the 95% confidence interval (95% CI) is provided to indicate the precision of the mean creep estimates across all groups. Creep differed significantly among the eight groups (one-way ANOVA: $F(7,32) = 1363.1$, $p < 0.001$); Holm-adjusted pairwise comparisons versus the unmodified control (M) were significant for all CaF_2-modified compositions (adjusted $p < 0.001$).

Table 5. Creep (%) of the investigated dental amalgam groups

Alloys	Mean Creep (%)	Mean SD	95% CI	Improvement (%)
SG43	1.11%	0.035	1.065 – 1.155	-
M	0.907%	0.016	0.892 – 0.922	-
M + 0.5% CaF_2	0.809%	0.001	0.808 – 0.810	10.8%
M + 1% CaF_2	0.620%	0.014	0.603 – 0.637	31.63%
M + 1.5% CaF_2	0.543%	0.002	0.541 – 0.545	40.13%
M + 2% CaF_2	0.407%	0.003	0.403 – 0.411	55.12%
M + 2.5% CaF_2	0.366%	0.015	0.349 – 0.383	57.62%
M + 3% CaF_2	0.288%	0.023	0.263 – 0.313	68.25%

3.6 Ion release test

3.6.1 Mercury ion release

Table 6 summarizes mercury release (Hg, ppb) for the reference groups (SG43 and M) and the CaF_2-modified specimens under the present test conditions. The master alloy (M) exhibited higher Hg release than SG43. Relative to M, all CaF_2-modified compositions showed lower Hg release, with a non-monotonic dependence on CaF_2 content. The minimum value occurred at 0.5 wt% CaF_2, whereas Hg release increased at higher contents but remained below M; notably, the 3 wt% CaF_2 group approached the SG43 reference.

Table 6. Mercury release (Hg, ppb) for the investigated dental amalgam groups under the present test conditions

Sample	Hg (ppb)
SG43	2.1533
M	4.2546
M + 0.5% CaF_2	0.0326
M + 1% CaF_2	0.1199
M + 1.5% CaF_2	0.1239
M + 2% CaF_2	0.7211
M + 2.5% CaF_2	0.4351
M + 3% CaF_2	2.1533

3.6.2 Fluoride ion release

Table 7 presents the fluoride ion release (F^-) measured after 30 days of immersion in artificial saliva at 37 ± 1 °C for the CaF_2-modified groups (0.5–3%). A clear decreasing trend was observed with increasing CaF_2 content: the measured F^- value decreased from 4.07 at 0.5% to 3.75 (1%), 3.50 (1.5%), 3.30 (2%), 3.05 (2.5%), and reached 2.80 at 3%. This concentration-dependent reduction indicates that higher CaF_2 additions were associated with lower fluoride release under the present test conditions, suggesting a more stable fluoride-containing surface/near-surface state and reduced ion leaching into the surrounding medium over prolonged immersion. The decrease in F^- release with increasing CaF_2 may reflect reduced leaching from a more stable fluoride-containing surface or near-surface layer and/or reduced effective CaF_2 exposure due to particle retention/agglomeration (i.e., a lower accessible surface area) under the present test conditions. Further time-resolved kinetic studies are warranted.

Table 7. Fluoride ion release (F^-) after 30 days of immersion in artificial saliva at 37 ± 1 °C

Sample	F^- (ppm)
M + 0.5% CaF_2	4.07
M + 1% CaF_2	3.75
M + 1.5% CaF_2	3.50
M + 2% CaF_2	3.30
M + 2.5% CaF_2	3.05
M + 3% CaF_2	2.80

4. ETHICAL CONSIDERATIONS

This study was conducted entirely in vitro using

commercially available dental amalgam (SG43), a laboratory-prepared master alloy (M), and CaF_2-modified formulations. No human participants, patient data, or animal subjects were involved; therefore, institutional ethical approval and informed consent were not required. All procedures followed established laboratory safety and good scientific practice. Because the materials contain mercury, handling and testing were performed under appropriate mercury-safety measures (adequate ventilation and suitable PPE), and all mercury-containing residues and contaminated consumables were collected and disposed of as hazardous waste in accordance with institutional and environmental regulations.

5. CONCLUSIONS

Within the limitations of the present in-vitro study, CaF_2 incorporation (0.5–3.0 wt%) modified the microstructure of the fabricated high-copper dental amalgam while preserving the characteristic set-amalgam phases ($\gamma1$–Ag_2Hg_3 and η–Cu_6Sn_5). XRD consistently showed retained CaF_2 reflections alongside the amalgam phases, and no additional reaction-derived crystalline phases were detected within the instrument's detection limits; complementary characterization supported the persistence of CaF_2-related signatures. Across the investigated window, compressive strength and hardness increased with CaF_2 content, whereas dimensional change and creep decreased, with the best overall load-bearing response observed at 3 wt% CaF_2 under the present testing conditions. Mercury release was minimized at 0.5 wt% CaF_2 under the present immersion protocol, whereas fluoride release varied with composition. Collectively, these findings indicate that CaF_2 enables tailoring a practical balance between ADA-standard physicomechanical performance and Hg/F^- release, and the preferred composition depends on the intended priority (maximal strengthening versus minimal Hg release).

However, these conclusions are restricted to the investigated CaF_2 window (0.5–3.0 wt%) and to the current specimen preparation and testing conditions. In addition, Hg and F^- release was evaluated using the stated immersion medium and duration; therefore, release behavior may differ under longer-term, cyclic, or clinically representative environments. Further studies should extend the composition range, implement longer-term/cyclic aging and corrosion protocols, and incorporate quantitative phase-fraction and microstructure metrics—together with increased sample sizes—to refine mechanistic interpretation and optimize the composition for specific clinical-performance targets.

ACKNOWLEDGMENT

I would like to thank my supervisor, Dr. Haydar Hassan Jamal Al-Deen, for the unwavering support and guidance in this research. I would like also to extend my gratitude to the Dean of the Materials Engineering College, Head Metallurgy Engineering Department and all the staff for their great efforts. I wish to express my deepest thanks to the staff and laboratories of the Metallurgical Department of the Materials Engineering College/University of Babylon.

REFERENCES

[1] Boțilă, M.R., Popa, D.L., Mercuț, R., Iacov-Crăițoiu, M.M., Scrieciu, M., Popescu, S.M., Mercuț, V. (2024). A finite element method study of stress distribution in dental hard tissues: Impact of access cavity design and restoration material. Bioengineering, 11(9): 878. https://doi.org/10.3390/bioengineering11090878

[2] Tobias, G., Chackartchi, T., Mann, J., Haim, D., Findler, M. (2024). Survival rates of amalgam and composite resin restorations from big data real-life databases in the era of restricted dental mercury use. Bioengineering, 11(6): 579. https://doi.org/10.3390/bioengineering11060579

[3] Osiro, O.A., Kariuki, D.K., Gathece, L.W. (2020). The Minamata convention on mercury and its implications for management of dental caries in low- and middle-income countries. International Dental Journal, 69(4): 247-251. https://doi.org/10.1111/idj.12461

[4] Kisumbi, B.K., Osiro, O.A., Gathece, L.W., Maina, S.W. (2025). Dental amalgam phase-down—Status, alternatives, strategies and preparedness for implementation: A review. International Journal of Dentistry, 2025(1): 6688410. https://doi.org/10.1155/ijod/6688410

[5] Estrich, C.G., Eldridge, L.A., Lipman, R.D., Araujo, M.W. (2023). Posterior dental restoration material choices in privately insured people in the United States, 2017 through 2019. The Journal of the American Dental Association, 154(5): 393-402. https://doi.org/10.1016/j.adaj.2023.02.005

[6] Fidancioğlu, Y.D., Alkurt Kaplan, S., Mohammadi, R., Gönder, H.Y. (2025). Three-dimensional finite element analysis (FEM) of tooth stress: The impact of cavity design and restorative materials. Applied Sciences, 15(17): 9677. https://doi.org/10.3390/app15179677

[7] Niknam, E., Naffakh-Moosavy, H. (2025). A review of current status, challenges, and future of the metallic amalgams. Journal of Hazardous Materials Advances, 18: 100732. https://doi.org/10.1016/j.hazadv.2025.100732

[8] Ali, M.S., Mehatlaf, A.A. (2025). Dental amalgam alloy reinforced with alumina and copper nanoparticles. Annales de Chimie. Science des Materiaux, 49(4): 349-355. https://doi.org/10.18280/acsm.490402

[9] Yazicioglu, O., Ucuncu, M.K., Aydin, S. (2025). Comparative measurement of mercury release values from amalgam restorations with different surface numbers: An in vitro study. Applied Sciences, 15(12): 6646. https://doi.org/10.3390/app15126646

[10] Liu, D., Xie, X., Roscher, J., Holze, R. (2020). A comparative study of the corrosion stability of dental amalgams with electrochemical impedance measurements. Materials and Corrosion, 71(6): 949-955. https://doi.org/10.1002/maco.201911468

[11] Moxon, R., Xu, Z., Tettey, F., Chris-Okoro, I., Kumar, D. (2024). Dental metal matrix composites: The effects of the addition of titanium nanoparticle particles on dental amalgam. Materials, 17(7): 1662. https://doi.org/10.3390/ma17071662

[12] Bourgi, R., Doumandji, Z., Cuevas-Suárez, C.E., Ben Ammar, T., Laporte, C., Kharouf, N., Haikel, Y. (2025). Exploring the role of nanoparticles in dental materials: A comprehensive review. Coatings, 15(1): 33. https://doi.org/10.3390/coatings15010033

[13] Mitwalli, H., Balhaddad, A.A., AlSahafi, R., Oates, T.W., Melo, M.A.S., Xu, H.H.K., Weir, M.D. (2020). Novel CaF2 nanocomposites with antibacterial function and

fluoride and calcium ion release to inhibit oral biofilm and protect teeth. Journal of Functional Biomaterials, 11(3): 56. https://doi.org/10.3390/jfb11030056
[14] Di Lauro, A., Di Duca, F., Montuori, P., Dal Piva, A.M.D.O., Tribst, J.P.M., Borges, A.L.S., Ausiello, P. (2023). Fluoride and calcium release from alkasite and glass ionomer restorative dental materials: In vitro study. Journal of Functional Biomaterials, 14(2): 109. https://doi.org/10.3390/jfb14020109
[15] Ritwik, A., Saju, K.K. (2021). Development of calcium fluoride thin film on Ti-6Al-4V material by a dip coating process with an intermediate shellac layer for biocompatible orthopedic applications. International Journal of Mechanical and Materials Engineering, 16(1): 7. https://doi.org/10.1186/s40712-021-00130-w
[16] Gallusi, G., Libonati, A., Piro, M., Di Taranto, V., Montemurro, E., Campanella, V. (2021). Is dental amalgam a higher risk factor rather than resin-based restorations for systemic conditions? A systematic review. Materials, 14(8): 1980. https://doi.org/10.3390/ma14081980
[17] No, S. (1977). Alloy for Dental Amalgam. JADA, 95, 614. https://doi.org/10.14219/jada.archive.1977.0123
[18] Torres, C.R.G., Patil, S., Batista, G.R. (2019). Amalgam restorations. In Modern Operative Dentistry: Principles for Clinical Practice, pp. 373-409. https://doi.org/10.1007/978-3-030-31772-0_11
[19] Black, J., Hastings, G. (2016). Chapter 1d Dental Restoration Materials. In Handbook of Biomaterial Properties, pp. 191-203. https://doi.org/10.1007/978-1-4939-3305-1_17
[20] Nakai, M., Niinomi, M. (2015). Dental Metallic Materials. In Advances in Metallic Biomaterials, pp. 251-281. https://doi.org/10.1007/978-3-662-46842-5_12
[21] Ismay, C., Kim, A.Y., Valdivia, A. (2025). Statistical Inference via Data Science: A Moderndive into R and the Tidyverse. Chapman and Hall/CRC. https://doi.org/10.1201/9781032724546

NOMENCLATURE

CI	confidence interval
d	specimen diameter, mm
F^-	fluoride ion
gf	gram-force, g
h	height, mm
Hg	mercury, ppb
HV	vickers hardness
n	number of specimens/replicates
SD	standard deviation
t	time
T	temperature, ℃
wt%	weight percent
x	individual measured value
$\bar{X}$	arithmetic mean
λ	X-ray wavelength, Å

Greek symbols

β	Ag_4Sn intermetallic phase
γ	Ag_3Sn intermetallic phase
γ_1	Ag_2Hg_3 phase
ε	Cu_3Sn intermetallic phase
η	Cu_6Sn_5 phase
η′	Cu – Sn reaction-product
2θ	XRD diffraction angle, degrees